Molecular Cancer

RESEARCH

Open Access

Inhibition of 6-phosphogluconate dehydrogenase suppresses esophageal squamous cell carcinoma growth and enhances the anti-tumor effects of metformin via the AMPK/mTOR pathway

Bei Wang[1,2,3†], Zixuan Wang[5,6†], Zini Zhou[4,5], Gui Liu[4,7], Zhenyuan Jiang[5,6], Mingyue Zheng[2,3] and Wei Geng[1,4,5,7*]

Abstract

Metabolic reprogramming plays a pivotal role in the development and progression of tumors. Tumor cells rely on glycolysis as their primary energy production pathway and effectively utilize biomolecules generated by the pentose phosphate pathway (PPP) for efficient biosynthesis. However, the role of 6-phosphogluconate dehydrogenase (6PGD), a crucial enzyme in the PPP, remains unexplored in esophageal squamous cell carcinoma (ESCC). In this study, we observed a significant upregulation of 6PGD expression in ESCC tissues, which correlated with an unfavorable prognosis among patients. The experiments demonstrated that knockdown of 6PGD induces oxidative stress and suppresses ESCC cell proliferation. Mechanistically, this is achieved through AMPK activation and subsequent inhibition of downstream mTOR phosphorylation. Moreover, physcion has been found to inhibit 6PGD activity and exert its anti-ESCC effect via the AMPK/mTOR pathway. Subsequently, we conducted both in vitro and in vivo experiments to validate the anticancer efficacy of combining metformin, an AMPK activator, with physcion. The results demonstrated a significantly enhanced inhibition of ESCC growth. This study elucidates the impact of 6PGD on ESCC cell proliferation along with its underlying molecular mechanisms, highlighting its potential as a therapeutic target for ESCC. Furthermore, we investigated a novel approach for improved anti-tumor therapy involving physcion and metformin. These findings will contribute new insights to clinical treatment strategies for ESCC while providing a theoretical foundation for developing molecular targeted therapies.

Keywords Pentose phosphate pathway, 6-phosphogluconate dehydrogenase, Esophageal squamous cell carcinoma, Physcion, Metformin

†Bei Wang and Zixuan Wang contributed equally to this work.

*Correspondence:
Wei Geng
weihuo2001@163.com

Full list of author information is available at the end of the article

Introduction

Esophageal cancer (EC) is a highly aggressive gastrointestinal malignancy that poses a substantial threat to human health. According to the 2022 global cancer statistics, EC ranks 14th in incidence and 8th in mortality. Moreover, China bears more than half of the global burden in terms of both cases and deaths attributed to EC, making it one of the regions with the highest prevalence worldwide [1, 2]. The primary treatments for EC include surgery and chemoradiotherapy; however, the average 5-year survival rate remains approximately 10–15% [3, 4]. Poor prognosis in patients is significantly influenced by tumor recurrence and metastasis, while current chemotherapy regimens have demonstrated limited efficacy in managing this disease [5]. Despite advancements in targeted therapies for various cancers, progress in treating EC has been relatively modest [6]. Therefore, identifying key therapeutic targets and developing effective drugs are critical to addressing this clinical challenge.

Metabolic reprogramming represents a critical hallmark of tumor development and progression. This phenomenon is attributed to the aberrant metabolic pathways observed in tumors compared to normal tissues, which contribute to accelerated tumor growth and metastasis [7–12]. The "Warburg effect," characterized by increased glycolysis and compromised mitochondrial aerobic metabolism, plays a key role in tumor metabolic reprogramming [13–15]. Moreover, the pentose phosphate pathway (PPP) exhibits increased activity in tumor cells, leading to the production of nicotinamide adenine dinucleotide phosphate (NADPH) and ribose 5-phosphate (R-5-P), both of which are essential precursors for biochemical synthesis and facilitate DNA replication and tumor proliferation [16–18]. 6-phosphogluconate dehydrogenase (6PGD) plays a crucial role in the PPP, and alterations in its expression levels directly impact the generation of metabolic intermediates, consequently influencing the malignant progression of tumors [19, 20]. Although 6PGD is frequently overexpressed in various types of cancer tissues and has been associated with poor prognosis, its role in esophageal squamous cell carcinoma (ESCC) remains inadequately explored.

The present study aims to investigate the potential correlation between aberrant expression of 6PGD in ESCC tissues and patients' prognosis. Additionally, this research seeks to validate the impact of downregulating 6PGD expression or inhibiting its activity on ESCC cell proliferation. Furthermore, the molecular mechanism underlying its action is elucidated. Subsequently, the potential therapeutic value of combining inhibitors targeting 6PGD with metformin for treating ESCC was investigated.

Results

6PGD is elevated in ESCC tissues and correlates with an unfavorable prognosis

The expression of 6PGD in ESCC tissues was investigated using data from the TCGA database. The results showed a significant increase in 6PGD expression compared to normal tissues (Fig. 1A). To investigate the impact of differential 6PGD expression on overall survival (OS) in ESCC patients, the Kaplan-Meier Plotter database was used. The optimal cut-off value for 6PGD expression was determined at the peak hazard ratio (HR) and the minimum *p*-value (Additional file 1: Figure S1A), and the results indicated that patients with low 6PGD expression exhibited extended survival durations (Fig. 1B). RT-qPCR was conducted to quantify the mRNA levels of 6PGD in tumor and adjacent tissues from 12 ESCC patients, revealing a significant upregulation in tumor tissues (Fig. 1D). Western blot analysis was performed on tumor and adjacent tissues from another 6 patients, confirming a significant elevation in 6PGD protein levels in tumor tissues (Fig. 1C). Immunohistochemistry (IHC) analysis was conducted on tissue microarrays (TMAs) containing samples from 89 to 91 ESCC patients, respectively. Ultimately, based on the cut-off values derived from two TMAs using time-dependent receiver operating characteristic (ROC) curve analysis, 77 and 103 patients were stratified into high-expression and low-expression groups (Additional file 1: Figure S1B and C). Representative images depicting high and low expression levels of 6PGD are presented in Fig. 1E. Survival analysis demonstrated that elevated levels of 6PGD were significantly associated with poorer prognosis (Fig. 1F). Further stratification into distinct clinical subgroups demonstrated that increased expression of 6PGD consistently served as a risk factor across all analyzed subgroups (Additional file 1: Figure S1D). Univariate and multivariate analyses demonstrated the independent prognostic significance of 6PGD in patients with ESCC (Additional file 1: Table S1). These findings suggest that aberrant expression of 6PGD may play a role in the malignant progression of ESCC.

Knockdown of 6PGD suppresses the proliferation of ESCC cells

The expression of 6PGD was assessed in ESCC cell lines and normal esophageal epithelial cells using RT-qPCR and western blot analyses. Results revealed upregulation of 6PGD expression in ESCC cell lines (Fig. 2A and B). Knockdown of 6PGD was achieved in KYSE-30 and KYSE-410 cells using shRNA, as confirmed by RT-qPCR and western blot analyses (Fig. 2C and D). As a result of 6PGD knockdown, the generation of NADPH was markedly diminished in both cell lines (Fig. 2E). Furthermore, depletion of 6PGD impeded the proliferation of ESCC cells, as demonstrated by the CCK-8 assay for

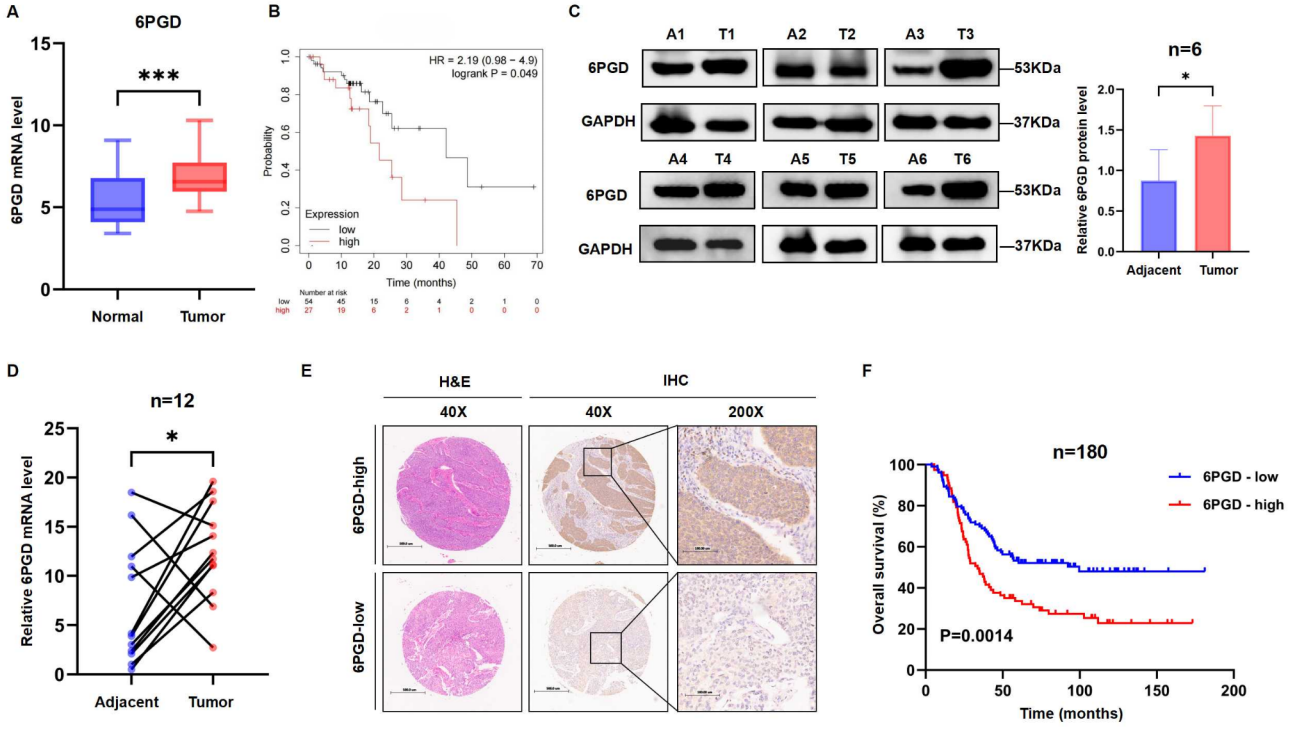

Fig. 1 The up-regulation of 6PGD in ESCC tissues is associated with a poor prognosis. (**A**) Expression levels of 6PGD in ESCC tissues and non-tumor esophageal tissues in the TCGA database. (**B**) Survival analysis based on 6PGD for ESCC using the Kaplan-Meier Plotter ($n=81$, $P=0.049$). (**C**) 6PGD protein level in tumor and adjacent tissues detected by Western blotting ($n=6$). (**D**) The mRNA level of 6PGD in tumor and adjacent tissues quantified by RT–qPCR ($n=12$). (**E**) Representative H&E and IHC staining images of tumor tissues from TMAs comprising samples collected from ESCC patients. Scale bar for 40× magnification: 500 μm; scale bar for 200× magnification: 100 μm. (**F**) Overall survival difference between the groups with high and low expression of 6PGD ($n=180$, $P=0.0014$). *$P<0.05$, ***$P<0.001$

cell viability and the colony formation assay for clone generation (Fig. 2F and G). To further validate these findings, we also established a stable 6PGD-knockdown TE-1 cell line (Additional file 1: Figure S2A and B). The results indicated that the knockdown of 6PGD markedly decreased NADPH production and significantly reduced cell viability (Additional file 1: Figure S2C and D). In contrast, the knockdown of 6PGD in normal esophageal epithelial cells had minimal impact on cellular viability and proliferation (Additional file 1: Figure S3). These observations suggest that elevated 6PGD expression may promote ESCC cell proliferation.

Reactive Oxygen Species (ROS) are crucial molecules generated during oxidative stress. Excessive ROS accumulation disrupts the cellular oxidation-reduction balance, leading to selective damage or death of tumor cells [21, 22]. 6PGD is a vital enzyme in the PPP. Downregulating its expression reduces NADPH production, diminishing ROS clearance and achieving anti-tumor effects. To test this hypothesis, we investigated changes in intracellular ROS levels following the knockdown of 6PGD. The findings revealed a significant elevation in cellular ROS levels after 6PGD knockdown compared to control cells (Fig. 2H, Additional file 1: Figure S2E). Cell cycle analysis confirmed an increase in the proportion of cells in the G0/G1 phase following 6PGD knockdown (Fig. 2I-K, Additional file 1: Figure S2G). It is well established that cyclin-dependent kinases (CDKs) play a pivotal role in regulating the cell cycle. Specifically, the complex formed by Cyclin E and CDK2 facilitates the smooth progression of cells through the G1/S checkpoint and into the S phase, thereby ensuring efficient DNA synthesis and promoting cellular proliferation. The Western Blot analysis revealed a significant reduction in CDK2 protein levels following 6PGD knockdown (Fig. 2L). This suggests that the transition from the G0/G1 phase to the S phase is impeded in 6PGD-depleted cells, leading to impaired nuclear DNA synthesis and consequently affecting cellular proliferative capacity. To further validate this finding, EdU staining experiments were conducted, which demonstrated that DNA synthesis was reduced in ESCC cells with 6PGD knockdown (Fig. 2M and N, Additional file 1: Figure S2F). Overall, these findings suggest that downregulating 6PGD disrupts cellular redox balance, impedes progression into the S phase of the cell cycle, slows down the DNA synthesis rate, and consequently inhibits cell proliferation.

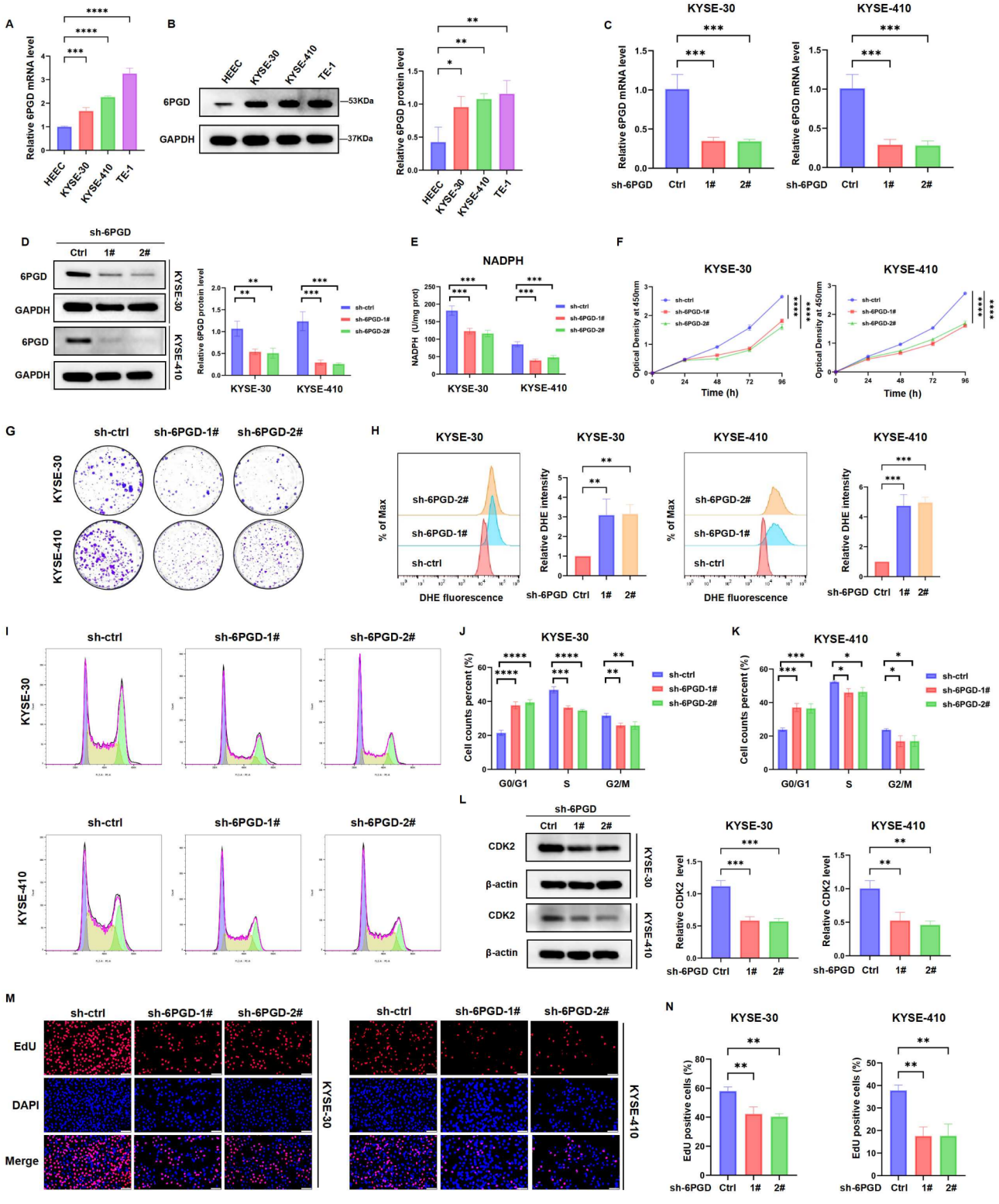

Fig. 2 (See legend on next page.)

(See figure on previous page.)

Fig. 2 Knockdown of 6PGD suppresses the proliferation of ESCC cells. (**A**, **B**) The mRNA and protein levels of 6PGD were evaluated using RT-qPCR and western blot analyses in ESCC cell lines and normal esophageal epithelial cells ($n = 3$, mean ± SD). (**C**, **D**) The knockdown efficiency of 6PGD in KYSE-30 and KYSE-410 cells was validated through RT-qPCR and western blot analyses ($n = 3$, mean ± SD). (**E**) The production of NADPH decreased following the knockdown of 6PGD ($n = 3$, mean ± SD). (**F**) CCK-8 assay was employed to assess the impact of 6PGD knockdown on the viability of KYSE-30 and KYSE-410 cells ($n = 3$, mean ± SD). (**G**) The colony-forming ability of ESCC cells undergoes alterations following the knockdown of 6PGD. (**H**) The knockdown of 6PGD in KYSE-30 and KYSE-410 cells resulted in an elevation of intracellular ROS levels ($n = 3$, mean ± SD). (**I-K**) The alterations in the cell cycle distribution of ESCC cells following the knockdown of 6PGD ($n = 3$, mean ± SD). (**L**) Western blot analysis revealed a reduction in the expression of CDK2 protein in ESCC cells following 6PGD knockdown ($n = 3$, mean ± SD). (**M**, **N**) The DNA synthesis capacity in ESCC cells following 6PGD knockdown was assessed using EdU staining assays ($n = 3$, mean ± SD); Scale bar, 100 μm. $^{*}P < 0.05$, $^{**}P < 0.01$, $^{***}P < 0.001$, $^{****}P < 0.0001$; ns means non-significant

6PGD regulates cell proliferation by modulating the AMPK/mTOR pathway

To further elucidate the molecular mechanisms underlying 6PGD-mediated ESCC proliferation, RNA-seq analysis was conducted on 6PGD knockdown cells and control cells. The results demonstrated that in KYSE-30 cells with 6PGD knockdown, 551 genes were significantly downregulated while 1,102 genes were significantly upregulated (Fig. 3A). KEGG enrichment analysis revealed significant enrichment of downregulated genes in the mTOR signaling pathway, as well as substantial alterations in pathways related to ribosome biogenesis, cell cycle regulation, and DNA replication (Fig. 3B). These findings suggest that 6PGD plays a pivotal role in regulating cellular biosynthesis. Additionally, RNA sequencing was performed on KYSE-410 cells with 6PGD knockdown and control cells, and KEGG enrichment analysis also indicated significant enrichment of downregulated genes in the mTOR signaling pathway (Additional file 1: Figure S4A and B). Previous studies have demonstrated that 6PGD influences ACC1 phosphorylation via the LKB1-AMPK pathway, thereby promoting fatty acid synthesis in tumor cells [23]. AMPK serves as a pivotal regulator of cellular energy homeostasis. Upon sensing low energy levels, the AMPK pathway becomes activated, which subsequently inhibits anabolic processes and enhances catabolic activities [24, 25]. mTOR functions as a downstream effector of AMPK and primarily governs protein synthesis. The activation of AMPK results in the suppression of mTOR activity, leading to reduced protein synthesis [26]. Consequently, we propose that ESCC cell proliferation is modulated by 6PGD through the regulation of the AMPK/mTOR signaling pathway. Through western blot analysis, a marked increase in AMPK phosphorylation and a significant reduction in mTOR phosphorylation were observed in KYSE-30 and KYSE-410 cells following 6PGD knockdown (Fig. 3C, Additional file 1: Figure S4C).This study showed that 6PGD knockdown led to a substantial increase in cellular ROS levels, indicating that ROS may serve as an upstream signaling molecule to activate the AMPK pathway. To further investigate this mechanism, we employed N-acetylcysteine (NAC), a well-characterized ROS scavenger [27, 28], to mitigate intracellular ROS production. The results demonstrated that NAC effectively reduced intracellular ROS levels elevated by 6PGD knockdown and restored cell viability inhibited by 6PGD knockdown (Fig. 3D **and E**, Additional file 1: Figure S4D and E). Western blot analysis indicated that AMPK and mTOR phosphorylation levels were restored to baseline levels (Fig. 3F **and G**, Additional file 1: Figure S4F and G). Additionally, CCK-8 assays revealed that Compound C, an AMPK inhibitor, could diminish the inhibitory effect of 6PGD knockdown on cell viability (Fig. 3H, Additional file 1: Figure S4H). Furthermore, as the phosphorylation level of AMPK decreased, the phosphorylation level of mTOR showed a corresponding increase (Fig. 3I **and J**, Additional file 1: Figure S4I and J). Administration of the mTOR agonist MHY1485 led to a significant enhancement in mTOR phosphorylation in 6PGD knockdown cells, thereby mitigating the suppression of cell viability (Fig. 3K-M, Additional file 1: Figure S4K-M). These results suggest that targeting 6PGD modulates the AMPK/mTOR pathway, which in turn inhibits tumor cell proliferation.

Physcion inhibits ESCC cell proliferation through the suppression of 6PGD activity

The active compound physcion, extracted from Rhubarb, has demonstrated inhibitory effects on tumor proliferation and metastasis [29, 30]. Prior research has shown that physcion selectively targets 6PGD and effectively suppresses the proliferation of lung cancer, breast cancer, and head and neck cancer cells [31–33]. In this study, we observed a significant increase in the activity of 6PGD in ESCC cells, which was subsequently significantly decreased following physcion treatment (Fig. 4A, Additional file 1: Figure S5A). Furthermore, the increase in the dosage of the drug led to a progressive decline in cell viability (Fig. 4B, Additional file 1: Figure S5B). The clone formation assay demonstrated a diminished capacity for cell cloning in the physcion-treated group (Fig. 4C). Flow cytometry analysis revealed a dose-dependent elevation in cellular ROS levels following physcion treatment (Fig. 4D, Additional file 1: Figure S5C and D), which resulted in G0/G1 phase cell cycle arrest and decreased expression of CDK2 protein (Fig. 4E **and F**, Additional file 1: Figure S5G and H). The EdU staining assay confirmed that physcion significantly inhibited DNA synthesis in ESCC cells (Fig. 4G, Additional file 1: Figure S5E and F). To further investigate the impact of physcion on

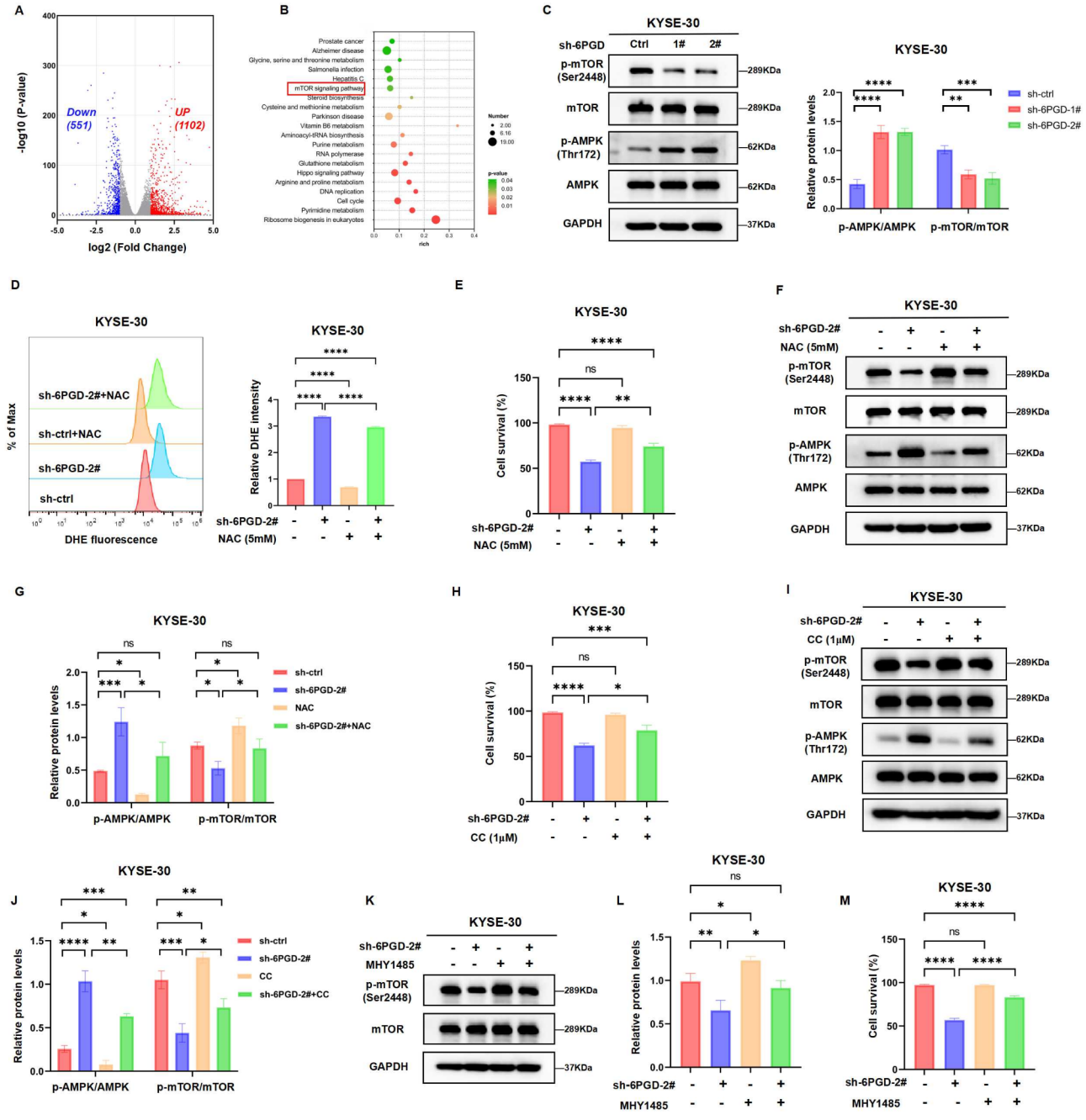

Fig. 3 6PGD regulates cell proliferation by modulating the AMPK/mTOR pathway. (**A**) The volcano plot shows changes in gene expression after 6PGD knockdown in KYSE-30 cells. (**B**) KEGG pathway analysis was performed on the down-regulated genes following 6PGD knockdown in KYSE-30 cells. (**C**) Western blot analysis showed increased p-AMPK and decreased p-mTOR levels after 6PGD knockdown in KYSE-30 cells ($n = 3$, mean ± SD). (**D**) The elevation in intracellular ROS levels induced by 6PGD knockdown was reversed by NAC treatment ($n = 3$, mean ± SD). (**E**) NAC mitigates the reduction in cell viability caused by 6PGD knockdown ($n = 3$, mean ± SD). (**F**, **G**) Western blot analysis showed that NAC treatment effectively reversed the changes in phosphorylation levels of AMPK and mTOR ($n = 3$, mean ± SD). (**H**) The AMPK inhibitor (Compound C) mitigated the reduction in cell viability caused by 6PGD knockdown ($n = 3$, mean ± SD). (**I**, **J**) Compound C reversed the increased phosphorylation of AMPK caused by 6PGD knockdown, and subsequently restored the phosphorylation levels of mTOR ($n = 3$, mean ± SD). (**K**, **L**) The mTOR agonist MHY1485 mitigated the reduction in mTOR phosphorylation induced by 6PGD knockdown ($n = 3$, mean ± SD). (**M**) MHY1485 alleviated the suppressive effect of 6PGD knockdown on cellular viability ($n = 3$, mean ± SD). $^{*}P < 0.05$, $^{**}P < 0.01$, $^{***}P < 0.001$, $^{****}P < 0.001$; ns means non-significant

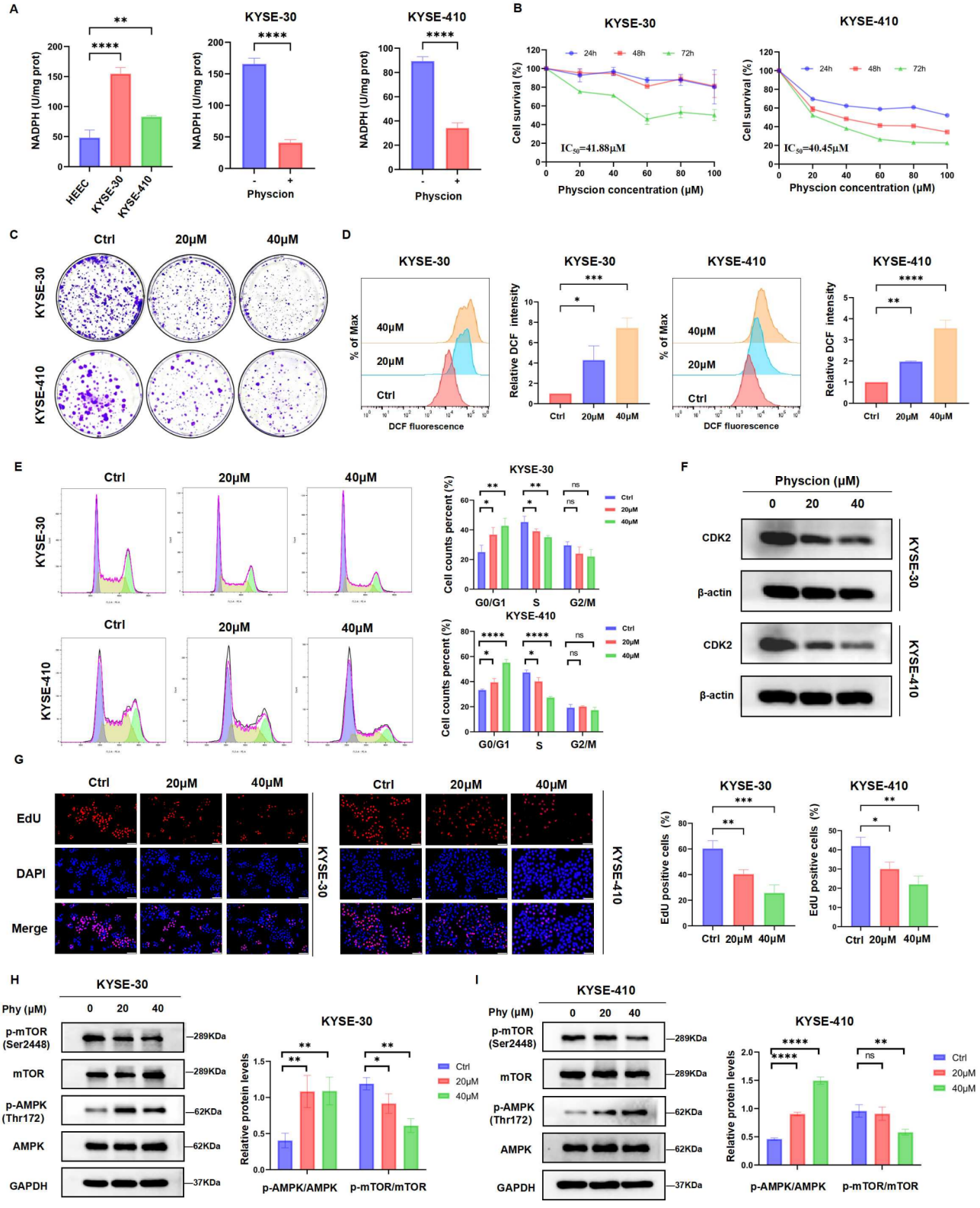

Fig. 4 (See legend on next page.)

(See figure on previous page.)

Fig. 4 Physcion inhibits ESCC cell proliferation through the suppression of 6PGD activity. (**A**) The production of NADPH is upregulated in KYSE-30 and KYSE-410 cells, but it is significantly reduced after treatment with physcion (40μM) for 24 h ($n = 3$, mean ± SD). (**B**) The cell viability of KYSE-30 and KYSE-410 cells was evaluated after treatment with various concentrations of physcion for 24 to 72 h ($n = 3$, mean ± SD). (**C**) KYSE-30 and KYSE-410 cells were treated with physcion for 72 h, followed by an additional 10 days of incubation to assess colony formation. (**D**) Intracellular ROS levels in ESCC cells fluctuated after 48 h of physcion treatment ($n = 3$, mean ± SD). (**E**) Cell cycle changes in KYSE-30 and KYSE-410 cells were observed after exposure to physcion for 48 h ($n = 3$, mean ± SD). (**F**) Western blot analysis revealed a reduction in CDK2 protein expression in ESCC cells following physcion treatment. (**G**) The effect of physcion on DNA synthesis in ESCC cells was detected using an EdU staining assay ($n = 3$, mean ± SD); Scale bar: 100 μm. (**H**, **I**) Western blot analysis was performed to evaluate changes in p-AMPK and p-mTOR protein expression following physcion treatment ($n = 3$, mean ± SD). *$P < 0.05$, **$P < 0.01$, ***$P < 0.001$, ****$P < 0.0001$; ns means non-significant

ESCC cell growth through its interaction with 6PGD, we conducted follow-up experiments in KYSE-30 and KYSE-410 cells with 6PGD knockdown. The results demonstrated that the inhibitory effect of physcion on cell proliferation was abolished. No significant differences were observed in cell viability, intracellular ROS levels, cell cycle distribution, or DNA synthesis compared to control cells (Additional file 1: Figure S6). These findings suggest that physcion inhibits the proliferation of ESCC cells by targeting 6PGD. Western blot analysis further demonstrated that physcion upregulates p-AMPK and downregulates p-mTOR, which is consistent with the effects observed following 6PGD knockdown (Fig. 4H **and I**). Therefore, physcion may represent a promising therapeutic candidate for ESCC treatment.

ROS inhibitor mitigates the anticancer effects of physcion on ESCC

To investigate whether the elevation of ROS is the primary mechanism by which physcion inhibits the proliferation of ESCC cells, NAC was administered as a pre-treatment before physcion application. The results showed that NAC partially reversed the elevation of ROS induced by physcion (Fig. 5A **and B**). Cell proliferation was then assessed using the CCK-8 assay and EdU staining. The findings revealed that pre-treatment with NAC increased cell viability and the proportion of EdU-positive cells (Fig. 5C-F). These results suggest that suppressing ROS accumulation could enhance DNA synthesis and counteract the inhibitory effect of physcion on cell proliferation. Additionally, western blot analysis demonstrated that NAC can reverse the changes in the AMPK/mTOR pathway caused by physcion (Fig. 5G-J).

The combination of Metformin and physcion enhances the Inhibition of ESCC cell proliferation

Numerous studies have reported the anti-tumor activity of metformin; however, achieving effective anti-tumor effects requires prolonged exposure to high doses of metformin, which presents significant treatment risks and hinders its practical clinical application [34–36]. Utilizing a drug combination represents a valuable clinical treatment strategy for reducing the effective dosage of metformin while maintaining its efficacy. Given that metformin acts as an AMPK agonist and physcion inhibits tumor proliferation by activating the AMPK signaling pathway, we hypothesized that combining metformin with physcion may yield enhanced effects. Based on this hypothesis, we conducted in vitro experiments to explore the combined effects of these two drugs. The results of the CCK-8 assay indicated that the viability of KYSE-30 and KYSE-410 cells progressively decreased with increasing concentrations of metformin and prolonged exposure duration (Fig. 6A **and B**). Moreover, the combination of metformin and physcion resulted in a significantly greater reduction in cell viability compared to either agent used individually (Fig. 6C-F). The combination index (CI) values were all less than 1, indicating a potential synergistic effect (Fig. 6G, Additional file 1: Table S2). Clone formation and EdU staining assays revealed that low-dose metformin has no significant effect on cell proliferation; however, when combined with physcion, it significantly enhanced the inhibitory effects on cell growth (Fig. 6H-J). Furthermore, ROS levels were significantly increased in the combination group compared to single-drug treatments (Fig. 6K **and L**). Western blot results also confirmed higher AMPK phosphorylation levels following drug combinations, while mTOR phosphorylation levels were lower (Fig. 6M **and N**).

Effects of physcion combined with Metformin on the growth of ESCC in vivo

To investigate the in vivo effects of physcion combined with metformin, we established tumor models in BALB/c nude mice utilizing KYSE-30 and KYSE-410 cell lines, respectively. The results showed no significant changes in nude mouse weight under single or combined drug administration (Fig. 7A **and B**). Compared to the control group, the mice subjected to drug intervention exhibited a significant reduction in tumor volume, which was further reduced in the combined treatment group (Fig. 7C-H). Western blot results demonstrated significant changes in AMPK and mTOR phosphorylation levels following treatments with physcion and metformin, particularly in the combined group (Fig. 7I). H&E staining as well as Ki-67 IHC analysis were conducted on sections obtained from KYSE-30 tumor-bearing nude mice. The results revealed that the combination group exhibited the most significant reduction in Ki-67 expression levels within tumor tissue (Fig. 7J), indicating a pronounced

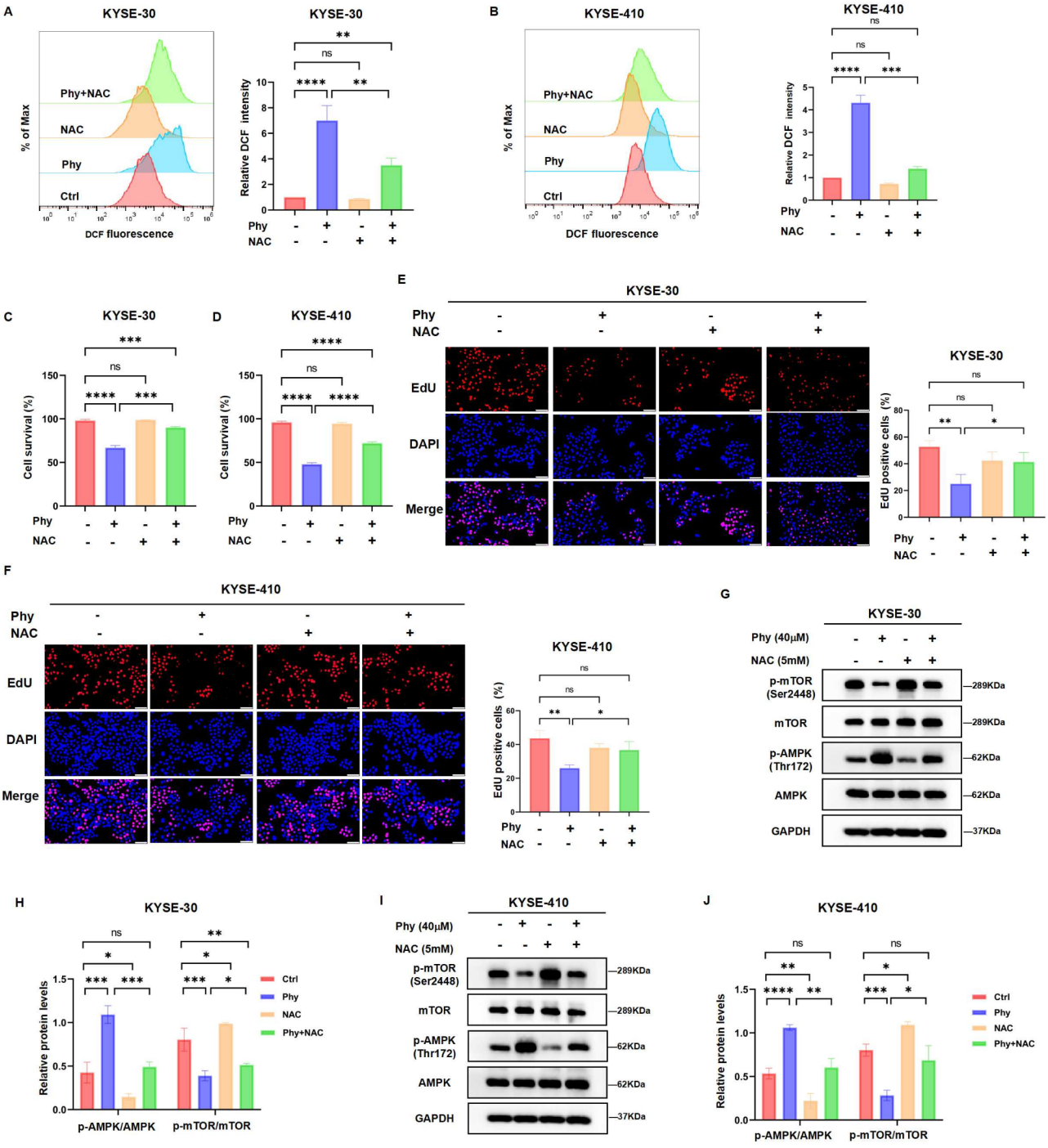

Fig. 5 ROS inhibitor mitigates the anticancer effects of physcion on ESCC. (**A**, **B**) Pre-treatment with NAC (5 mM) attenuated the physcion-induced increase in ROS levels in KYSE-30 and KYSE-410 cells ($n = 3$, mean ± SD). (**C**, **D**) CCK-8 assay showed that NAC effectively counteracted physcion's inhibitory effect on ESCC cell viability ($n = 3$, mean ± SD). (**E**, **F**) The rescue effect of NAC on physcion-induced inhibition of DNA synthesis was assessed using the EdU staining assay ($n = 3$, mean ± SD); Scale bar: 100 μm. (**G-J**) The western blot analysis showed that NAC pre-treatment effectively reversed the impact of physcion on the AMPK/mTOR pathway ($n = 3$, mean ± SD). $^{*}P < 0.05$, $^{**}P < 0.01$, $^{***}P < 0.001$, $^{****}P < 0.0001$; ns means non-significant

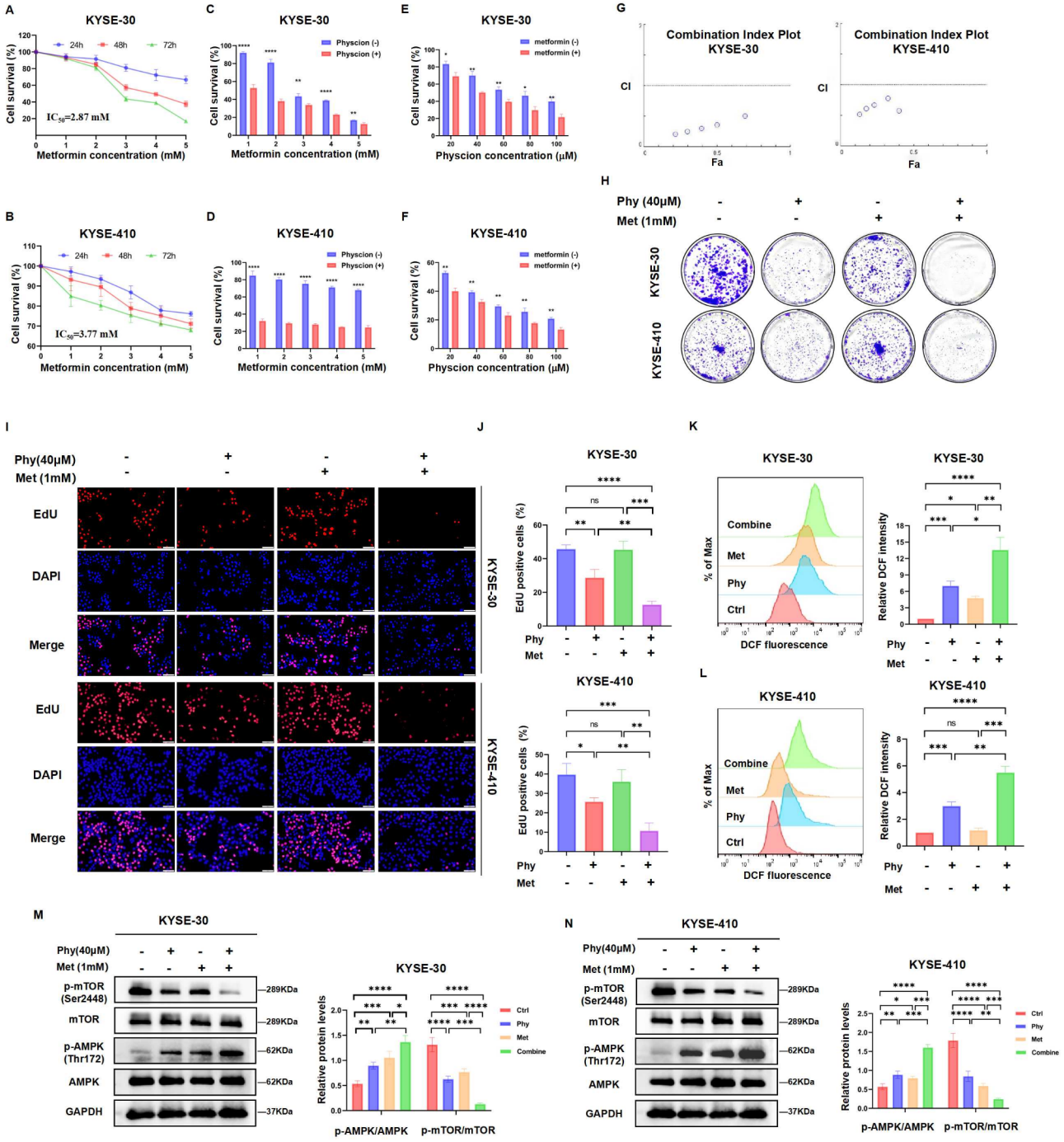

Fig. 6 The combination of metformin and physcion enhances the inhibition of ESCC cell proliferation. (**A**, **B**) The cell viability of KYSE-30 and KYSE-410 cells was evaluated after treatment with various concentrations of metformin for 24 to 72 h ($n = 3$, mean ± SD). (**C**, **D**) A CCK-8 assay was used to detect the effects of different concentrations of metformin alone or in combination with 40 μM physcion on the viability of ESCC cells treated for 72 h ($n = 3$, mean ± SD). (**E**, **F**) The effects of varying concentrations of physcion alone or in combination with 1 mM metformin on the viability of KYSE-30 and KYSE-410 cells were examined ($n = 3$, mean ± SD). (**G**) The synergistic effect of physcion and metformin in ESCC cells was investigated using Compusyn software. (**H**) The impact of the combination of physcion (40 μM) and metformin (1mM) on clonal formation in ESCC cells. (**I**, **J**) The EdU staining assay was employed to assess the inhibitory effect of physcion (40 μM) on DNA synthesis in ESCC cells treated with metformin (1mM) for 48 h ($n = 3$, mean ± SD); Scale bar: 100 μm. (**K**, **L**) Flow cytometry detected the effect of physcion combined with metformin on intracellular ROS levels ($n = 3$, mean ± SD). (**M**, **N**) The modulation of the AMPK/mTOR pathway in response to physcion and metformin treatments, either alone or in combination, was evaluated ($n = 3$, mean ± SD). *$P < 0.05$, **$P < 0.01$, ***$P < 0.001$, ****$P < 0.0001$; ns means non-significant

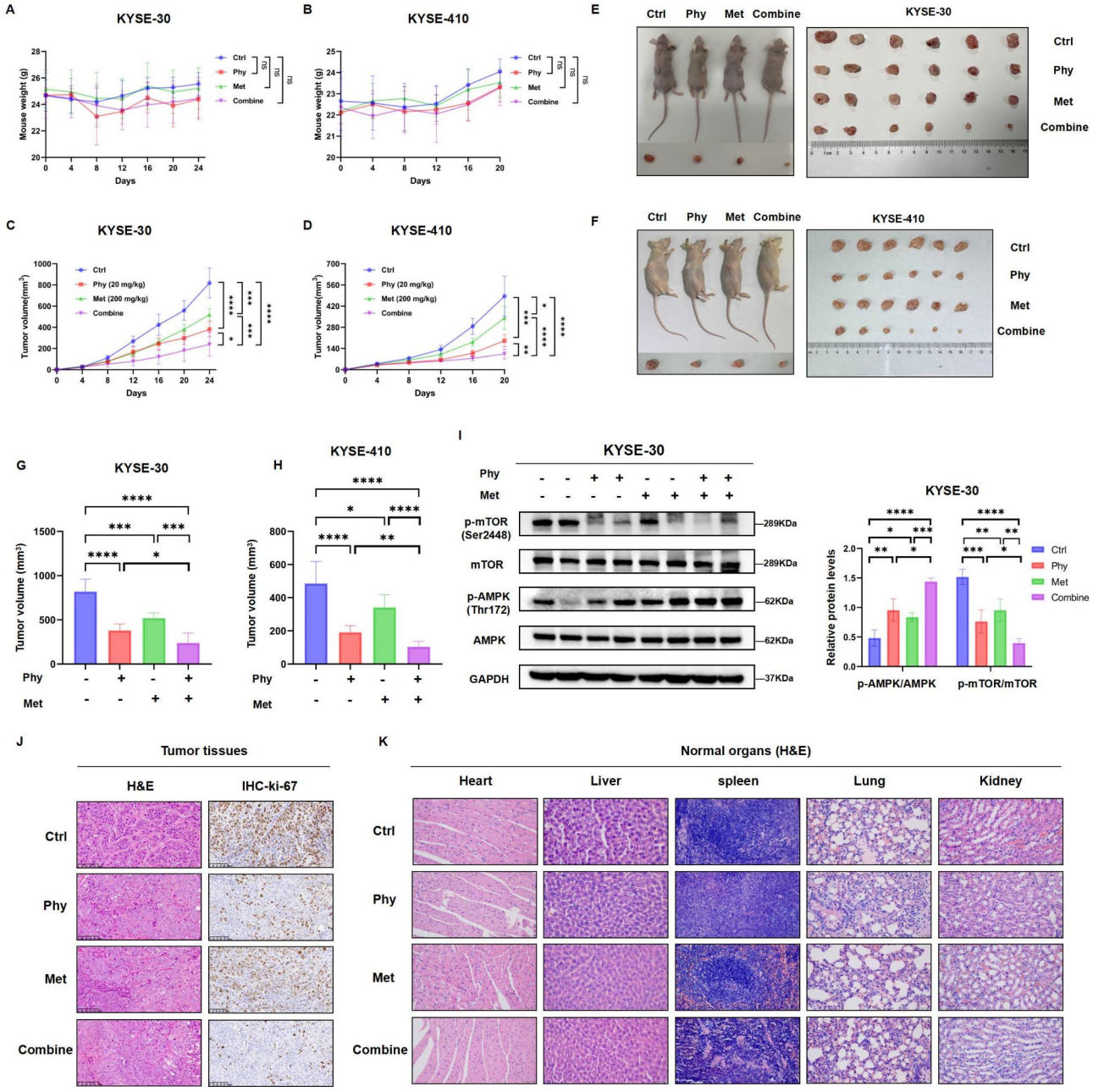

Fig. 7 Effects of physcion combined with metformin on the growth of ESCC in vivo. The changes in body weight (**A**, **B**) and tumor volume (**C**, **D**) in nude mice after administration of physcion (20 mg/kg) and metformin (200 mg/kg) as single drugs or in combination. (**E-H**) The differences in tumor volume among the treatment groups ($n = 6$). (**I**) The differential expression of p-AMPK and p-mTOR in tumor tissues across various groups was assessed using western blot analysis ($n = 3$, mean ± SD). (**J**) H&E staining as well as Ki-67 IHC analysis were conducted on sections obtained from KYSE-30 tumor-bearing nude mice; Scale bar: 100 μm. (**K**) H&E staining was performed to assess organ damage across different treatment groups, Scale bar: 100 μm. *$P < 0.05$, **$P < 0.01$, ***$P < 0.001$, ****$P < 0.0001$; ns means non-significant

inhibition of tumor proliferation. Subsequent H&E staining was performed on normal organs from each group of nude mice. Neither monotherapy with metformin nor monotherapy with physcion, nor their combination, resulted in noticeable damage to normal organs (Fig. 7K). These findings suggest that combining physcion and metformin can modulate ESCC growth through activation of the AMPK/mTOR pathway without inducing toxic effects.

Discussion

The energy supply of tumor cells primarily relies on glycolysis for ATP generation, while the PPP is utilized for cellular synthesis by producing necessary biomolecules

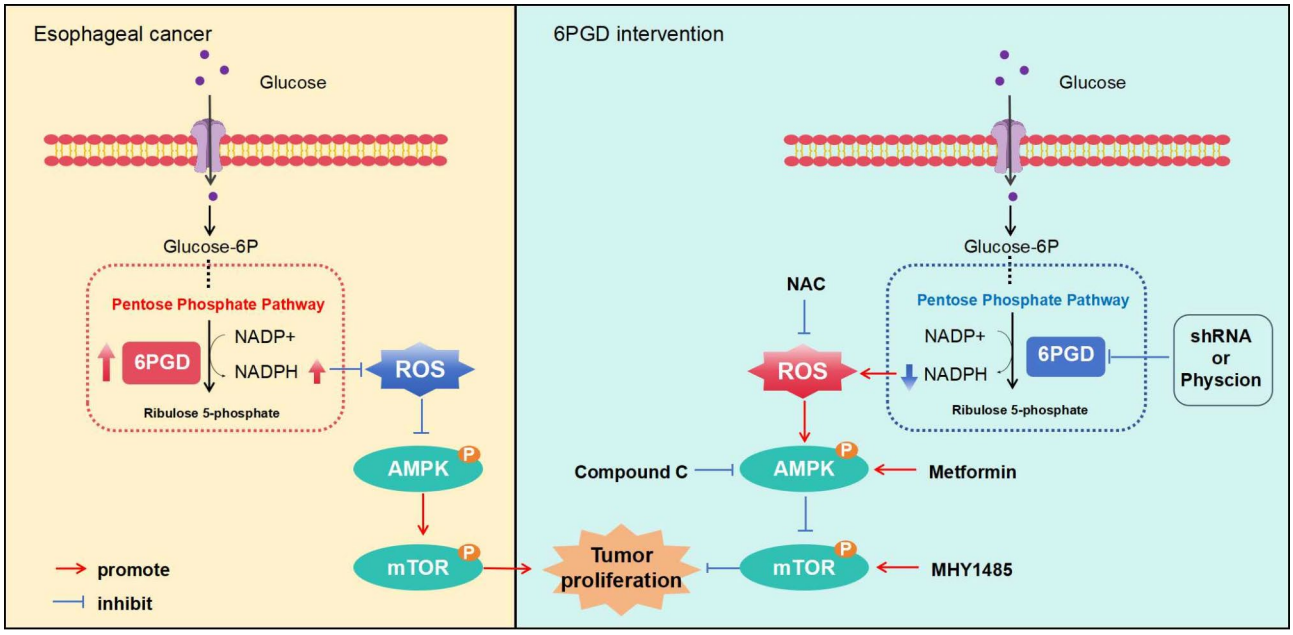

Fig. 8 Graphical representation of the mechanism by which 6PGD modulates the proliferation of ESCC

[37, 38]. Therefore, targeting key metabolic enzymes in the PPP can inhibit DNA replication by reducing the production of biosynthesis substrates, which has important practical implications for controlling tumor cell proliferation. 6PGD plays a crucial role in the PPP and is significantly upregulated in various cancers. The present study initially examined tissue samples from patients and found higher expression of 6PGD in ESCC tissues compared to adjacent normal tissues. Furthermore, IHC analysis of TMAs confirmed that elevated 6PGD expression was associated with a poorer prognosis. Subsequent in vitro experiments showed that knocking down 6PGD increased cellular ROS levels, leading to cell cycle arrest at the G0/G1 phase, inhibition of DNA synthesis, and decreased cell proliferation. RNA sequencing and KEGG enrichment analysis revealed that genes significantly down-regulated following 6PGD knockdown were predominantly enriched in the mTOR signaling pathway, which is crucial for mediating cell survival and proliferation. These findings validate the potential therapeutic strategy for ESCC by targeting 6PGD.

Natural products, characterized by their distinctive chemical structures and biological activities, have emerged as a crucial source for the development of molecularly targeted therapeutics. Physcion, derived from rhubarb, Cassia obtusifolia, and other medicinal plants, inhibits 6PGD activity and suppresses lung cancer and leukemia cell proliferation by regulating ACC1 to impede fatty acid synthesis [29]. It induces autophagy in nasopharyngeal carcinoma cells [32]. In cervical cancer, physcion inhibits AKT activation, increases intracellular oxidative stress and DNA damage, thereby inducing cell apoptosis and necrosis [39, 40]. Additionally, it reduces the migration ability of cervical cancer cells by decreasing RhoA and Rac1 activity [41], as well as regulates the epithelial-mesenchymal transition (EMT) process by inhibiting SOX2 transcription factors in colorectal cancer cells [42]. This study presents initial evidence of physcion's inhibitory effect on the proliferation of ESCC cells. It also investigates the impact of this compound on cellular functions in both wild-type and 6PGD stably low-expressed ESCC cell lines. The findings validate that physcion effectively suppresses cell proliferation by inhibiting 6PGD activity. Mechanistically, the knockdown of 6PGD or intervention with physcion reduces NADPH production, leading to ROS accumulation. This induces oxidative stress, activates the AMPK pathway, and inhibits the mTOR pathway, thus suppressing cell proliferation (Fig. 8). Unlike previous reports, physcion did not significantly induce apoptosis in this study, which may be attributed to the varying drug responsiveness observed across different tumor types (Additional file 1: Figure S7). In this investigation, only two concentrations (20 μM and 40 μM) were employed for intervention, both of which were confirmed to regulate ESCC cell proliferation through cell cycle arrest. This suggests that modulation of the cell cycle is the predominant mechanism by which physcion affects ESCC cell proliferation. However, the potential of higher concentrations to induce apoptosis remains an area that warrants further investigation. In investigating metastasis, we conducted wound healing assays and Transwell migration assays to evaluate the impact of 6PGD on cellular migration. The results indicated that both 6PGD knockdown and physcion

treatment could suppress the migratory capacity of ESCC cells. However, these differences were not statistically significant (Additional file 1: Figure S8).

Based on the aforementioned research, we propose that physcion inhibits ESCC cell proliferation through AMPK activation. Previous studies have demonstrated metformin's effectiveness as an AMPK activator and its anti-tumor mechanism involving the regulation of the AMPK/mTOR pathway. Therefore, in this study, we conducted an in-depth investigation into the anti-tumor efficacy of combining physcion with metformin for the treatment of ESCC.Both in vivo and in vitro studies have demonstrated that the combination of metformin and physcion significantly enhances anti-tumor efficacy. While previous research has established metformin's capability to inhibit ESCC growth, its clinical application is limited by the necessity for high dosages. Our findings suggest that the anti-tumor effects of metformin are markedly potentiated when administered in conjunction with physcion. This combination therapy represents a promising novel approach and strategy for clinical intervention.

This study also has some limitations. Firstly, the optimal combination dosing regimen of physcion and metformin has not been thoroughly investigated. Specifically, in vivo dosages and administration methods have not been validated through pharmacokinetic studies. Secondly, this study exclusively utilized cell line-derived xenotransplantation (CDX) models; future research should incorporate patient-derived xenotransplantation (PDX) models to enhance the robustness and translational relevance of the findings. Additionally, it remains unclear whether other pathways beyond the ROS-mediated AMPK/mTOR signaling pathway contribute to the regulation of ESCC cell proliferation. Future studies will delve deeper into these deficiencies and unresolved issues.

In summary, this study elucidates the critical role of 6PGD in promoting malignant progression in ESCC and provides insights into its underlying molecular signaling pathways. It was demonstrated that physcion effectively inhibits 6PGD, thereby suppressing ESCC growth. Moreover, the study explored the potential synergistic anti-tumor effects of combining metformin with physcion. Collectively, these findings not only offer a comprehensive understanding of targeting 6PGD as a therapeutic strategy for ESCC but also propose a promising combined treatment approach with significant potential for future clinical applications.

Materials and methods

Database analysis

A comprehensive and standardized pan-cancer dataset was retrieved from the UCSC Xena Browser (https://xenabrowser.net/). The expression levels of ENSG00000142657 (6PGD) across all samples were extracted, and the expression values were log2-transformed using log2(x + 0.001). We then conducted a differential expression analysis of 6PGD between ESCC tissues and adjacent normal tissues. Additionally, survival analysis of ESCC patients based on 6PGD expression was performed using the Kaplan-Meier Plotter database (https://kmplot.com/analysis/).

Human ESCC tissues

A total of 198 patients diagnosed with ESCC were included in this study. Among these, tissue samples from 18 patients were cryopreserved at -80 °C for subsequent RT-qPCR and Western blot analyses. Additionally, tissue samples from 180 patients were obtained from paraffin-embedded blocks stored in the pathology department for the construction of tissue microarrays (TMAs) and subsequent IHC analysis. All patients were pathologically diagnosed with ESCC and had not received neoadjuvant therapy. Fresh surgical specimens were promptly immersed in RNALater solution within 30 min post-excision, subsequently stored at 4 °C overnight, and then transferred to -80 °C for long-term preservation. For TMA construction, representative areas free of necrosis and hemorrhage were identified via H&E staining. Cylindrical tissue cores measuring 1 mm in diameter were extracted, embedded in paraffin wax, and sectioned into 3 μm thick slices. This study was conducted with the approval of the Ethics Committee of the Yancheng First People's Hospital (Approval number: 2022-K-016), and all patients provided written informed consent.

Cell lines and cultures

The normal human esophageal epithelial cells (HEEC) were purchased from Shanghai Meiwan Biotechnology Co., Ltd., while the ESCC cell lines (KYSE-30, KYSE-410, TE-1) were purchased from Wuhan procell Life Technology Co., Ltd. HEEC cells were cultured in MEM medium (L510KJ, BasalMedia Technologies, China), whereas KYSE-30, KYSE-410, and TE-1 were cultured in RPMI 1640 medium (L210KJ, BasalMedia Technologies, China). The cells were supplemented with 10% fetal bovine serum (FBS, PWL001, Meilunbio, China) and 1% penicillin/streptomycin solution (P/S, Meilunbio, China), and incubated at 37 °C with 5% CO_2.

Reagents

Physcion (HY-N0108), N-Acetylcysteine (HY-B0215), Compound C (HY-13418), MHY1485 (HY-B0795), dimethyl sulfoxide (DMSO, HY-Y0320), and cremophor EL (HY-Y1890) were purchased from MedChemExpress (MCE, USA). Metformin (S1741) was purchased from Beyotime Biotechnology (Beyotime, China). Physcion and N-Acetylcysteine were dissolved in DMSO for in vitro experiments, while physcion was dissolved

in cremophor EL for in vivo experiments, and metformin solution was prepared with diethylpyrocarbonate (DEPC)-treated water.

Real-time quantitative PCR (RT-qPCR)

Total RNA was extracted from tissues or cells using TRIzol reagent (Vazyme Biotech, China). The RNA samples were then purified and reverse-transcribed into cDNA using a reverse transcription kit (Vazyme Biotech, China). RT-qPCR analysis was performed using 2× Taq Pro Universal SYBR qPCR Master Mix (Vazyme Biotech, China). The relative expression levels of 6PGD were quantified using the 2^-ΔΔCT method, with GAPDH as an internal control. Primers for 6PGD and GAPDH were synthesized by Genscript Biotech Corporation (Genscript, China). The primer sequences are as follows: 6PGD: Forward: ATGGCCCAAGCTGACATCG; Reverse: AAAGCCGTGGTCATTCATGTT; GAPDH: Forward: ACAACTTTGGTATCGTGGAAGG; Reverse: GCCATCACGCCACAGTTTC.

Western blot analysis

The RIPA buffer (Beyotime, China) supplemented with protease inhibitors and phosphatase inhibitors was employed for the lysis of tissues or cells to extract total proteins. Subsequently, the protein samples were denatured by heating in 5× loading buffer (Beyotime, China) at 100 °C for 10 min and then separated via SDS-PAGE before being transferred onto PVDF membranes (Millipore, USA). Incubation with primary antibodies was carried out overnight at 4 °C. The primary antibodies used included anti-6PGD (1:1000, abs-110330, Absin), anti-AMPKα (1:1000, #2532, CST), anti-p-AMPK (1:1000, #2535, CST), anti-mTOR (1:1000, #2983, CST), anti-p-mTOR (1:1000, #5536, CST), anti-CDK2 (1:1000, A0094, ABclonal), anti-GAPDH (1:10000, AC002, ABclonal), and anti-β-actin (1:10000, AC026, ABclonal). Secondary antibodies, HRP-conjugated Goat anti-Rabbit (1:10000, AS014, ABclonal) and HRP-conjugated Goat anti-Mouse (1:10000, AS003, ABclonal), were then applied. Chemiluminescence detection was performed using ECL reagent (Meilunbio, China), and the protein bands were quantified using ImageJ software.

Immunohistochemistry (IHC)

The formalin-fixed and paraffin-embedded tissue sections underwent dewaxing and rehydration. Antigen retrieval was conducted by heating the sections in a microwave oven with sodium citrate buffer (Beyotime, China). Endogenous peroxidases were inhibited using 3% hydrogen peroxide (H_2O_2). The sections were subsequently incubated overnight at 4 °C with the following primary antibodies: anti-PGD (1:100, abs-110330, Absin) and anti-Ki67 (1:100, 27309-1-AP, Proteintech). The secondary antibody used was an HRP-conjugated goat anti-rabbit IgG (1:200, AS014, ABclonal). The sections were stained with 3,3'-diaminobenzidine tetrahydrochloride (DAB), followed by counterstaining of nuclei with hematoxylin, differentiation with acid alcohol, dehydration, clearing, and mounting.

To quantify 6PGD expression, three randomly selected fields were examined at a magnification of 200x per specimen. Using ImageJ software, the intensity of DAB staining was measured in each field. The average optical density (OD) value was calculated by dividing the total staining intensity by the stained area across all three fields. Ultimately, the expression level of 6PGD was determined based on this averaged OD value.

Transfection of cell lines

The interference plasmid targeting 6PGD and the empty vector were designed by Shanghai Genechem Co., Ltd. (Genechem, China). The specific sequences are as follows: sh-6PGD-1#: GACTTCTTTAAGTCAGCTG TT; sh-6PGD-2#: CCTGATTGAAATCACAGCCA A; sh-control: TTCTCCGAACGTGTCACGT. These sequences were inserted into the GV493 vector in the following order of elements: hU6-MCS-CBh-gcGFP-IRES-puromycin. Lentiviral transfection of KYSE-30 and KYSE-410 cells was performed according to the provided protocol. The experimental procedure is summarized as follows: Cells were seeded into a 6-well plate at a density of 5 × 10^4 cells per well. Twenty-four hours post-seeding, lentiviral transduction was initiated. After a transduction period of 12–16 h, the culture medium was replaced with fresh medium. Once cell confluence reached approximately 80%, a final concentration of 2 μg/mL puromycin was added to selectively eliminate non-transduced cells, thereby enriching the population of positively transduced cells. Knockdown efficiency was evaluated using RT-qPCR and western blot analysis.

RNA extraction and whole transcriptome sequencing

Total RNA was extracted from both the control cells and the sh-6PGD-2# cells using TRIzol reagent (Vazyme, China). Each group included three biological replicates. RNA sequencing was performed by Shanghai Bioprofile Co., Ltd. (Bioprofile, China) on the Illumina platform. Differentially expressed genes were identified, and subsequent Kyoto Encyclopedia of Genes and Genomes (KEGG) pathway enrichment analysis was conducted.

Cell counting Kit-8 (CCK-8) assay

The sh-control and sh-6PGD cells were individually seeded at a density of 3 × 10^3 cells per well in separate wells of a 96-well plate and incubated at 37 °C with 5% CO2. At 24, 48, 72, and 96 h post-seeding, 10 μl of CCK-8 reagent (Meilunbio, China) was added to each

well, followed by a two-hour incubation period before measuring the absorbance at 450 nm using a microplate reader. For in vitro drug intervention experiments, various concentrations of the compound were administered immediately after cell inoculation, and CCK-8 reagent was subsequently added at different time points to measure the absorbance.

The Compusyn software was utilized to calculate the Combination Index (CI) value for the interaction between physcion and metformin. A CI value less than 1 indicates a synergistic effect, while a CI value of 1 denotes an additive effect. Conversely, a CI value greater than 1 suggests an antagonistic effect.

Clone formation assay

The sh-control and sh-6PGD cells were seeded at a density of 600 cells per well in a 6-well plate, and the culture medium was refreshed every three days until visible colony formation was observed. For the drug intervention experiment, cells were treated with varying concentrations of the compound for 72 h and subsequently cultured for an additional 10 days. Thereafter, cells were fixed using 4% paraformaldehyde (Biosharp, China), stained with crystal violet (Solarbio, China), rinsed under running water, and air-dried.

Intracellular ROS detection assay

Transfected cells exhibiting a green fluorescent signal were incubated with the DHE working solution (KeyGEN, China) in serum-free medium. Upon cellular uptake, the DHE probe was oxidized by intracellular ROS to generate a red fluorescent product. Following a 30-minute incubation, cells were washed with PBS buffer to remove unbound probes, resuspended in PBS, and analyzed by flow cytometry to detect fluorescence intensity. The average fluorescence intensity, as calculated using FlowJo software, reflects the levels of intracellular ROS.

In the drug intervention experiment, cells were seeded at a density of 5 × 10^4 cells per well in 6-well plates and incubated for 24 h. Subsequently, various concentrations of the compound were administered, and the intracellular ROS levels were assessed after an additional 48-hour incubation. Cells were then incubated with the DCFH-DA working solution (Meilunbio, China) for 30 min, during which time the probe was oxidized to produce a green fluorescent signal. Fluorescence intensity was detected by flow cytometry, and the average fluorescence intensity was calculated using FlowJo software.

Cell cycle assay

The cells were washed with PBS and subsequently fixed in 70% ethanol at 4 °C overnight. Prior to flow cytometry analysis, the cells were incubated with the staining solution for 30 min as specified in the protocol of the Cell Cycle Staining Analysis Kit (Abbkine, China). The cell cycle distribution was analyzed using FlowJo software. For drug intervention experiments, cells were seeded at a density of 5 × 10^4 cells per well in 6-well plates and treated with varying concentrations of the compound. Cell cycle analysis was conducted on collected samples 48 h post-treatment.

EdU cell proliferation assay

ESCC sh-control and sh-6PGD cells were seeded in 96-well plates at a density of 3 × 10^3 cells per well. After 48 h, the cells were incubated with a 10 μM EdU solution prepared according to the protocol provided in the EdU cell proliferation kit (Abbkine, China) at 37 °C for 2 h. Subsequently, the cells were fixed with 4% paraformaldehyde and permeabilized using a 0.5% Triton X-100 solution (Phygene, China) for 15 min. The cells were then incubated with the Click-iT reaction mixture for an additional 30 min before nuclear labeling with DAPI was performed. Fluorescence microscopy was used to observe both EdU and DAPI staining, followed by image acquisition. Positive cell counts were conducted using ImageJ software. For drug intervention experiments, compounds were administered 24 h post-seeding, and EdU detection was performed after an additional 48-hour incubation period.

6PGD activity detection assay

The activity of 6PGD was assessed using the 6-Phosphogluconate Dehydrogenase Activity Assay Kit (Abbkine, China). Cells were collected, resuspended in Extraction Buffer, and subsequently lysed via sonication on ice. The lysates were centrifuged to collect the supernatant. Next, a reaction mixture consisting of 10 μL sample and 190 μL Working Solution was prepared in a 96-well plate. Absorbance at 340 nm was measured using a microplate reader at two time points: an initial reading (A1) taken over 10 s and a final reading (A2) taken after 3 min and 10 s. The change in absorbance (ΔAtest) was calculated as A2 - A1. Protein concentration was quantified using the BCA method. The specific activity of 6PGD was then determined using the following formula: 6PGD (U/mg protein) = 2144 × ΔAtest ÷ protein concentration. For the drug intervention experiments, cells were treated with the designated compounds 24 h post-seeding and subsequently incubated for an additional 24-hour period prior to assessing 6PGD activity.

Apoptosis detection assay

5 × 10^4 cells were seeded in each well of a six-well plate. Following an overnight incubation, the cells were exposed to different concentrations of the compound for 48 h. Subsequently, the cells were harvested and processed

according to the manufacturer's protocol for the Annexin V-FITC/PI Apoptosis Detection Kit (Elabscience, China). The proportion of apoptotic cells was then quantified using flow cytometry.

Cell mobility assay

For wound healing assays, cells were cultured in 12-well plates until confluence was achieved. Subsequently, a linear scratch was created vertically using a 200 µL pipette tip. The wells were then washed with PBS to remove cellular debris and replenished with serum-free medium. Microscopic images were captured at 0 h and 24 h post-scratch.

For the Transwell migration assay, 100 µL of serum-free cell suspension was seeded into the upper chamber ((8 µm pore size; Corning, USA), while 600 µL of medium supplemented with 10% fetal bovine serum was added to the lower chamber. After a 24-hour incubation period, cells on the upper surface of the membrane were removed, and those that had migrated to the lower surface were fixed and stained with crystal violet. Following PBS washes, images were captured using an inverted microscope.

Xenograft models

Forty-eight male BALB/c nude mice, aged 6 weeks, were obtained from Beijing Huafu Kang Biotechnology Co., Ltd. KYSE-30 cells (1.5 × 10^6 cells per 100 µL) and KYSE-410 cells (4.0 × 10^6 cells per 100 µL) were inoculated subcutaneously into the right dorsal region of each mouse. When the average tumor volume reached approximately 25 mm^3, the mice were randomized into distinct treatment groups. All medications were administered via gavage. For the physcion-treated group, the dosage was set at 20 mg/kg per administration; for the metformin-treated group, it was established at 200 mg/kg per administration. The combination treatment group received sequential gavage of both drugs at their respective dosages. Mice were orally administered these medications every other day, and their tumor dimensions and weights were monitored regularly. Humane euthanasia was performed when the tumor reached a maximum diameter of 20 mm or exhibited signs of ulceration, followed by cervical dislocation. All animal experimental procedures strictly adhered to the guidelines for animal welfare and were approved by the Ethics Committee for Medical Experimental Animals of Jiangsu Medical College (Approval number: XMLL-2022-853).

Statistic analysis

The Statistical Package for Social Sciences (SPSS) version 30.0 (IBM SPSS Statistics, Armonk, NY, USA) and GraphPad Prism version 9 (GraphPad Software Inc., San Diego, CA, USA) were utilized for statistical analysis and graphical representation. The optical density (OD) values from the immunohistochemistry (IHC) of 6-phosphogluconate dehydrogenase (6PGD) were evaluated using a receiver operating characteristic (ROC) curve to assess overall survival (OS) at three years post-surgery. The optimal cut-off value was determined to maximize both sensitivity and specificity. Survival differences between groups were analyzed using the Kaplan-Meier method. Clinical subgroup analysis was conducted using the Cox proportional hazards model. Continuous variables with normal distribution were compared using one-way analysis of variance (ANOVA) and independent samples t-tests. A p-value less than 0.05 was considered statistically significant.

Supplementary Information

The online version contains supplementary material available at https://doi.org/10.1186/s12943-025-02302-0.

Supplementary Material 1

Supplementary Material 2

Author contributions

WG designed and supervised this study; BW and ZW reviewed medical records, performed the experiments, prepared the figures and drafted the manuscript; ZZ, GL and ZJ participated in the collection of tissue samples and data analysis; MZ engaged in a comprehensive discussion and put forth innovative approaches for research methods. All authors read and approved the final manuscript.

Funding

This work was supported by the Jiangsu Province Traditional Chinese Medicine Science and Technology Development Program (YB2020079), the National Clinical Research Base of Traditional Chinese Medicine Project in Jiangsu Province, the China (JD2023SZX14), the Jiangsu Health Commission Project (Z2022016), the Yancheng Medical Innovation Team Fund, and the Key Specialty Construction Fund of Jiangsu Province.

Data availability

Data is provided within the manuscript or supplementary information files.

Declarations

Competing interests

The authors declare no competing interests.

Ethics approval and consent to participate

This study was conducted with the approval of the Ethics Committee of the Yancheng First People's Hospital (Approval number: 2022-K-016), and all patients provided written informed consent. The animal experimental procedures strictly adhered to the guidelines for animal welfare and were approved by the Ethics Committee for Medical Experimental Animals of Jiangsu Medical College (Approval number: XMLL-2022-853).

Author details

[1]Yancheng Key Laboratory of Molecular Epigenetics, The First people's Hospital of Yancheng, The Yancheng Clinical College of Xuzhou Medical University, 66 South People's Road, Yancheng 224000, Jiangsu, China
[2]School of Chinese Materia Medica, Nanjing University of Chinese Medicine, 138 Xianlin Road, Nanjing 210023, Jiangsu, China
[3]Drug Discovery and Design Center, State Key Laboratory of Drug Research, Shanghai Institute of Materia Medica, Chinese Academy of Sciences, 555 Zuchongzhi Road, Shanghai 201203, China

[4]Department of Radiotherapy, The First people's Hospital of Yancheng, The Yancheng Clinical College of Xuzhou Medical University, 66 South People's Road, Yancheng 224000, Jiangsu, China
[5]Xuzhou Medical University, 209 Tongshan Road, Xuzhou 221004, China
[6]Department of Radiotherapy, Jiangsu Cancer Hospital, The Affiliated Cancer Hospital of Nanjing Medical University, 42 Baizi Pavilion, Nanjing 210009, Jiangsu, China
[7]School of Medicine, Jiangsu University, 301 Xuefu Road, Zhenjiang 212013, Jiangsu, China

Received: 25 September 2024 / Accepted: 13 March 2025
Published online: 26 March 2025

References

1. An L, Li M, Jia Q. Mechanisms of radiotherapy resistance and radiosensitization strategies for esophageal squamous cell carcinoma. Mol Cancer. 2023;22(1):140.
2. Zhu H, et al. Esophageal cancer in China: practice and research in the new era. Int J Cancer. 2023;152(9):1741–51.
3. Puhr HC, Prager GW, Ilhan-Mutlu A. How we treat esophageal squamous cell carcinoma. ESMO Open. 2023;8(1):100789.
4. Li K, et al. Resected lymph nodes and survival of patients with esophageal squamous cell carcinoma: an observational study. Int J Surg. 2023;109(7):2001–9.
5. Yin J, et al. Neoadjuvant adebrelimab in locally advanced resectable esophageal squamous cell carcinoma: a phase 1b trial. Nat Med. 2023;29(8):2068–78.
6. Song Y, et al. ERK inhibitor: A candidate enhancing therapeutic effects of conventional chemo-radiotherapy in esophageal squamous cell carcinoma. Cancer Lett. 2023;554:216012.
7. Yang K, et al. The role of lipid metabolic reprogramming in tumor microenvironment. Theranostics. 2023;13(6):1774–808.
8. Faubert B, Solmonson A, DeBerardinis RJ. Metabolic reprogramming and cancer progression. Science, 2020. 368(6487).
9. Ohshima K, Morii E. Metabolic reprogramming of cancer cells during tumor progression and metastasis. Metabolites, 2021. 11(1).
10. Li Z, Zhang H. Reprogramming of glucose, fatty acid and amino acid metabolism for cancer progression. Cell Mol Life Sci. 2016;73(2):377–92.
11. Fhu CW, Ali A. Fatty acid synthase: an emerging target in cancer. Molecules, 2020. 25(17).
12. Stepka P, et al. Metabolic and amino acid alterations of the tumor microenvironment. Curr Med Chem. 2021;28(7):1270–89.
13. Lei P et al. Role of glucose metabolic reprogramming in breast cancer progression and drug resistance. Cancers (Basel), 2023. 15(13).
14. Vaupel P, Schmidberger H, Mayer A. The Warburg effect: essential part of metabolic reprogramming and central contributor to cancer progression. Int J Radiat Biol. 2019;95(7):912–9.
15. Liao M, et al. Targeting the Warburg effect: A revisited perspective from molecular mechanisms to traditional and innovative therapeutic strategies in cancer. Acta Pharm Sin B. 2024;14(3):953–1008.
16. Patra KC, Hay N. The Pentose phosphate pathway and cancer. Trends Biochem Sci. 2014;39(8):347–54.
17. Ghanem N, et al. The Pentose phosphate pathway in cancer: regulation and therapeutic opportunities. Chemotherapy. 2021;66(5–6):179–91.
18. Jiang P, Du W, Wu M. Regulation of the Pentose phosphate pathway in cancer. Protein Cell. 2014;5(8):592–602.
19. Sun M, et al. PRMT6 promotes tumorigenicity and cisplatin response of lung cancer through triggering 6PGD/ENO1 mediated cell metabolism. Acta Pharm Sin B. 2023;13(1):157–73.
20. Qiao R, et al. Critical role of 6-Phosphogluconate dehydrogenase in TAp73-Mediated cancer cell proliferation. Mol Cancer Res. 2023;21(8):825–35.
21. Moloney JN, Cotter TG. ROS signalling in the biology of cancer. Semin Cell Dev Biol. 2018;80:50–64.
22. Helfinger V, Schröder K. Redox control in cancer development and progression. Mol Aspects Med. 2018;63:88–98.
23. Yang X, Peng X, Huang J. Inhibiting 6-phosphogluconate dehydrogenase selectively targets breast cancer through AMPK activation. Clin Transl Oncol. 2018;20(9):1145–52.
24. Hsu CC, et al. AMPK signaling and its targeting in cancer progression and treatment. Semin Cancer Biol. 2022;85:52–68.
25. Li B, et al. Glucose restriction induces AMPK-SIRT1-mediated circadian clock gene per expression and delays NSCLC progression. Cancer Lett. 2023;576:216424.
26. González A, et al. The Yin and Yang of cellular nutrient sensing and growth control. Cell Metab. 2020;31(3):472–92.
27. Zheng L, et al. Piperlongumine synergistically enhances the antitumour activity of Sorafenib by mediating ROS-AMPK activation and targeting CPSF7 in liver cancer. Pharmacol Res. 2022;177:106140.
28. Song CF, et al. Hernandezine induces autophagic cell death in human pancreatic cancer cells via activation of the ROS/AMPK signaling pathway. Acta Pharmacol Sin. 2023;44(4):865–76.
29. Lin R, et al. 6-Phosphogluconate dehydrogenase links oxidative PPP, lipogenesis and tumour growth by inhibiting LKB1-AMPK signalling. Nat Cell Biol. 2015;17(11):1484–96.
30. Adnan M, et al. Physcion and physcion 8-O-β-D-glucopyranoside: natural anthraquinones with potential anticancer activities. Curr Drug Targets. 2021;22(5):488–504.
31. Zheng W, et al. Inhibition of 6-phosphogluconate dehydrogenase reverses cisplatin resistance in ovarian and lung cancer. Front Pharmacol. 2017;8:421.
32. Pang MJ, et al. Physcion, a naturally occurring anthraquinone derivative, induces apoptosis and autophagy in human nasopharyngeal carcinoma. Acta Pharmacol Sin. 2016;37(12):1623–40.
33. Zhang L, et al. The anti-breast cancer property of physcion via oxidative stress-mediated mitochondrial apoptosis and immune response. Pharm Biol. 2021;59(1):303–10.
34. Porper K, et al. A phase I clinical trial of dose-escalated metabolic therapy combined with concomitant radiation therapy in high-grade glioma. J Neurooncol. 2021;153(3):487–96.
35. Hua Y, et al. Metformin and cancer hallmarks: shedding new lights on therapeutic repurposing. J Transl Med. 2023;21(1):403.
36. Ding W, et al. Lower dose of Metformin combined with Artesunate induced autophagy-dependent apoptosis of glioblastoma by activating ROS-AMPK-mTOR axis. Exp Cell Res. 2023;430(1):113691.
37. Zhou Y, et al. Combined Inhibition of pyruvate dehydrogenase kinase 1 and lactate dehydrogenase a induces metabolic and signaling reprogramming and enhances lung adenocarcinoma cell killing. Cancer Lett. 2023;577:216425.
38. Kubik J et al. Targeting energy metabolism in cancer treatment. Int J Mol Sci, 2022. 23(10).
39. Wijesekara I, et al. Physcion from marine-derived fungus microsporum Sp. induces apoptosis in human cervical carcinoma HeLa cells. Microbiol Res. 2014;169(4):255–61.
40. Trybus W et al. Physcion induces potential anticancer effects in cervical cancer cells. Cells, 2021. 10(8).
41. Guo H, et al. Inhibiting 6-phosphogluconate dehydrogenase enhances chemotherapy efficacy in cervical cancer via AMPK-independent Inhibition of RhoA and Rac1. Clin Transl Oncol. 2019;21(4):404–11.
42. Han YT, et al. Physcion inhibits the metastatic potential of human colorectal cancer SW620 cells in vitro by suppressing the transcription factor SOX2. Acta Pharmacol Sin. 2016;37(2):264–75.

Publisher's note